

# Effective Field Theory for Rydberg Polaritons

M. J. Gullans,<sup>1</sup> Y. Wang,<sup>1</sup> J. D. Thompson,<sup>2</sup> Q.-Y. Liang,<sup>2</sup> V. Vuletić,<sup>2</sup> M. D. Lukin,<sup>3</sup> and A. V. Gorshkov<sup>1</sup>

<sup>1</sup>*Joint Quantum Institute and Joint Center for Quantum Information and Computer Science, National Institute of Standards and Technology and University of Maryland, College Park, Maryland 20742, USA*

<sup>2</sup>*Physics Department, Massachusetts Institute of Technology, Cambridge, Massachusetts 02138, USA*

<sup>3</sup>*Physics Department, Harvard University, Cambridge, Massachusetts 02138, USA*

We study non-perturbative effects in  $N$ -body scattering of Rydberg polaritons using effective field theory (EFT). We develop an EFT in one dimension and show how a suitably long medium can be used to prepare shallow  $N$ -body bound states. We then derive the effective  $N$ -body interaction potential for Rydberg polaritons and the associated  $N$ -body contact force that arises in the EFT. We use the contact force to find the leading order corrections to the binding energy of the  $N$ -body bound states and determine the photon number at which the EFT description breaks down. We find good agreement throughout between the predictions of EFT and numerical simulations of the exact two and three photon wavefunction transmission.

PACS numbers: 42.50.Nn, 32.80.Ee, 34.20.Cf, 42.50.Gy

Photons can be made to strongly interact by dressing them with atomic Rydberg states under conditions of electromagnetic induced transparency (EIT) [1–3]. Probing such Rydberg polaritons in the few-body limit, recent experiments were able to observe non-perturbative effects including the formation of bound states [4], single-photon blockade [5–7] and transistors [8–10], and two-photon phase gates [11]. Theoretical work on quantum nonlinear optics with Rydberg polaritons has focused on two-body effects or dilute systems [2–5, 12–17]; however, these theoretical methods often fail in dense systems with more than two photons.

Effective field theory (EFT) aims to describe low energy physics without resorting to a microscopic model at short distances or high energies [18]. In few-body systems, it is a useful approach to describe particle scattering and bound states when the momentum  $k$  involved is much less than the inverse range of the interactions [19, 20]. At the two-body level, the EFT depends only on the scattering length  $a_2$ . For scattering at momenta  $ka_2 \ll 1$ , one can solve the EFT perturbatively [20, 21]. However, describing unitarity ( $a_2 \rightarrow \infty$ ) or bound states requires inclusion of all orders in perturbation theory, which can be re-summed, provided the EFT parameters are properly renormalized [22, 23].

In this Letter, we develop an EFT for dispersive  $N$ -body scattering of Rydberg polaritons. We calculate the two-photon transmission and compare to numerical simulations, finding good agreement when the photon separation is less than the EIT group delay. We then show how a long one dimensional (1d) medium can be used to prepare shallow  $N$ -body bound states. We derive the  $N$ -body interaction potential that arises from Rydberg blockade. We show how these potentials give rise to a contact forces in the EFT, which lead to perturbative corrections to the  $N$ -body binding energy up to a critical value of  $N$ , past which the EFT breaks down.

A schematic of a Rydberg polariton transmission ex-

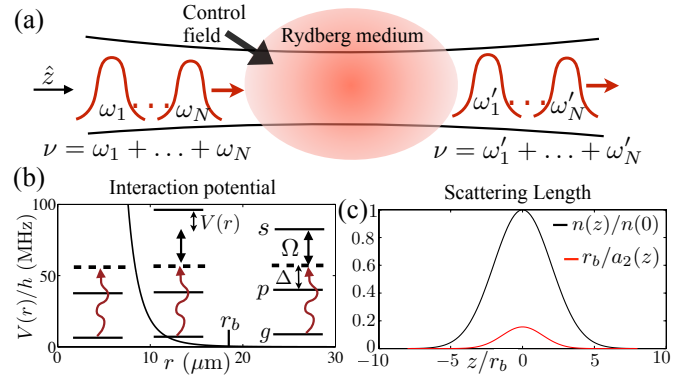


FIG. 1: (a) Rydberg polariton transmission experiment: an atomic cloud is probed with a few-photon beam, focused into a 1d channel, and a classical control field. Under dispersive conditions, the total energy  $\hbar\nu$  and number  $N$  of probe photons are conserved. (b) Interaction potential  $V(r) = C_6/r^6$  for two  $100\text{S}_{1/2}$  Rydberg states in  $^{87}\text{Rb}$ . The range is given by the blockade radius  $r_b$ . (Inset) Level diagram of an interacting atom for different  $r$ . (c) Dimensionless density  $n(z)/n(0) = \exp(-z^2/2\sigma_{ax}^2)$  and inverse scattering length  $r_b/a_2(z)$  for  $\sigma_{ax} = 36 \mu\text{m}$ ,  $r_b = 18 \mu\text{m}$ ,  $OD = 25$ ,  $\Omega/2\pi = 5 \text{ MHz}$ , and  $\Delta/2\pi = 20 \text{ MHz}$ .

periment is shown in Fig. 1(a) [14]. A spatially inhomogeneous atomic cloud is probed with a classical control field, with frequency  $\omega_c$  and Rabi frequency  $\Omega$ , and a few-photon probe beam focused into a 1d channel. The control and probe beams are configured for EIT on a two-photon resonance from the ground state  $|g\rangle$  to a Rydberg state  $|s\rangle$  via an intermediate state  $|p\rangle$ . We analyze the dispersive limit where the detuning of the control field  $\Delta = \omega_{ps} - \omega_c$  is much greater than the  $p$ -state halfwidth  $\gamma$ ; here  $\omega_{ab}$  is the atomic transition frequency from  $|a\rangle$  to  $|b\rangle$ . For large enough atomic density  $n(z)$ , the probe photons transform into Rydberg polaritons upon entering the medium because the collective, single-photon Rabi

frequency of the probe  $g_c(z) = [6\pi\gamma c^3 n(z)/\omega_{gp}^2]^{1/2}$  is much greater than  $\Omega$  [24]. We use the dimensionless measure of the density given by the resonant optical depth  $OD = \int dz [g_c(z)]^2 / 2\gamma c$ .

Consider two Rydberg states interacting through the van der Waals potential  $V(r) = C_6/r^6$ . This interaction is strong enough that a single Rydberg excitation modifies the optical response over a region large compared to the optical wavelength (see Fig. 1(b) and inset). The size of this region is given by the blockade radius  $r_b$ , defined by the condition that  $V(r_b)$  is equal to the off-resonant EIT linewidth  $2\Omega^2/|\Delta|$  [14, 25].

To see how these effects lead to strong photon-photon interactions, one can use a gedanken experiment where one photon (polariton) is held at fixed position  $z$ , then any photon that passes by will pick up a nonlinear phase shift  $\varphi(z) \approx [g_c(z)]^2 r_b / c\Delta$ ; here we assume  $g_c(z)$  varies slowly over  $r_b$ . For atomic densities achievable with laser-cooled atoms ( $n \gtrsim 10^{12} \text{ cm}^{-3}$ ), this nonlinear phase shift can be a sizable fraction of  $\pi$  [4]. An alternative metric is the two-body scattering length  $a_2$ , which was mapped out for Rydberg polaritons in a uniform medium in Ref. [12]. For an inhomogeneous medium, we can similarly define a local scattering length  $a_2(z)$ . For small  $\varphi(z)$ ,  $a_2(z) \approx (3/\pi)r_b/[\varphi(z)]^2$ . We show in the supplemental material that  $a_2(z)$  is well defined when the density varies slowly over  $r_b$  [26]. Figure 1(c) shows  $a_2(z)$  calculated for a Gaussian density profile with parameters similar to recent experiments [4].

In the absence of interactions, the propagation of Rydberg polaritons is captured by the local EIT dispersion relation [24, 26]

$$q(\omega, z) = \frac{\omega}{c} \left( 1 + \frac{[g_c(z)]^2}{\Omega^2 - \omega(\Delta + \omega)} \right), \quad (1)$$

where  $\omega = \omega_\ell - \omega_0$  is the detuning of the probe frequency  $\omega_\ell$  from the two-photon resonance  $\omega_0 = \omega_{gs} - \omega_c$ . The electric field of the probe evolves as  $E(\omega, z) = E(\omega, z_0) \exp[i\omega_0(z - z_0)/c + i \int_{z_0}^z dz' q(\omega, z')]$ . For a sufficiently slowly varying density, we can define a local group velocity  $v_g(z) = c/(1 + [g_c(z)]^2/\Omega^2)$  and effective mass  $m(z) = -\hbar\Omega^2/2\Delta[v_g(z)]^2$  by solving Eq. (1) for  $\omega$  and expanding near  $q = 0$ :  $\omega \approx v_g(z)q + \hbar q^2/2m(z)$  [24, 27].

These parameters define the Lagrangian density for the Rydberg polariton EFT

$$\mathcal{L} = \hat{\psi}^\dagger \left[ i\hbar\partial_t - i\hbar v_g(z)\partial_z - \frac{\hbar^2\partial_z^2}{2m(z)} \right] \hat{\psi} - \frac{\hbar^2\hat{\psi}^\dagger\hat{\psi}^2}{m(z)a_2(z)}, \quad (2)$$

where  $[\hat{\psi}(t, z), \hat{\psi}^\dagger(t, z')] = \delta(z - z')$  and  $\hat{\psi}$  is a single component field because the interactions only occur between  $|s\rangle$  states [12, 26]. Outside the medium,  $\hat{\psi}$  is the quantum field for the probe photons, while inside it corresponds to the Rydberg polariton field.

Despite its relative simplicity compared to the microscopic model [26], the theory is still difficult to solve because it has  $z$ -dependent parameters combined with second derivatives in  $z$ . To overcome this we define a new EFT with time and space exchanged via the local transformation  $(t, z) \rightarrow (z/v_g(z), tv_g(z))$ . Such a transformation is justified by the contact form of the interaction and has been used to study propagation of quantum light in nonlinear optical fibers [28–30]. For the steady state transmission with a uniform density, this transformation is equivalent to the rotated boundary conditions used in Ref. [4]. The resulting EFT is

$$\mathcal{L} = \hat{\psi}^\dagger \left[ i\hbar v_g(z)\partial_z - i\hbar\partial_t - \frac{\hbar^2\partial_t^2}{2m(z)[v_g(z)]^2} \right] \hat{\psi} - \frac{\hbar^2\kappa(z)}{m(z)[v_g(z)]^2} \hat{\psi}^\dagger\hat{\psi}^2, \quad (3)$$

where  $[\hat{\psi}(z, t), \hat{\psi}^\dagger(z, t')] = \delta(t - t')$  and we defined  $\kappa(z) = v_g(z)/a_2(z)$ . In Eq. (3) the second derivative is now in  $t$  rather than  $z$ , which makes it easier to account for the  $z$ -dependence of the EFT parameters. In particular, Eq. (3) gives rise to propagation equations akin to a time-dependent Schrödinger equation

$$-i\hbar v_g(z)\partial_z \hat{\psi}(z, t) = \int dt' [\mathcal{H}(z, t'), \hat{\psi}(z, t)], \quad (4)$$

where  $\mathcal{H}(z, t)$  is given by the last three terms in Eq. (3).

*Benchmarking the EFT.*—We now compare the predictions of the EFT for the two-photon transmission with numerical simulations of the exact wavefunction propagation [26]. We take a steady-state probe input on the two-photon resonance with parameters similar to Fig. 1(c), where  $a_2(z) > 0$  and the medium supports a single two-body bound state. We use the coordinates  $T = (t_1 + t_2)/2$  and  $\tau = t_1 - t_2$ , where  $t_{1(2)}$  are the time coordinates of the two polaritons. To find the transmission we use techniques from time-dependent quantum mechanics. We expand the wavefunction at every  $z$  in the eigenbasis [4]

$$\psi(z, T, \tau) = c_b(z)\psi_b(z, \tau) + \int_0^\infty \frac{d\omega}{2\pi} c_\omega(z)\psi_\omega(z, \tau), \quad (5)$$

where  $\psi_b = \sqrt{\kappa(z)}e^{-\kappa(z)|\tau|}$  is the local bound state,  $\psi_\omega = [e^{i\omega|\tau|} + b_\omega(z)e^{-i\omega|\tau|}]/\sqrt{2}$  are the local scattering states,  $b_\omega(z) = [i\omega + \kappa(z)]/[i\omega - \kappa(z)]$ , and  $\partial_T\psi = 0$  because we are on two-photon resonance. We use a uniform input  $\psi(0, T, \tau) = 1$  to set the initial conditions for  $c_{b(\omega)}$ . The propagation equations for  $c_{b(\omega)}$  are found from Eq. (4).

The results are shown in Fig. 2(a,b) for a Gaussian density profile  $n(z) \propto \exp[-(z - L/2)^2/2\sigma_{ax}^2]$  with a cutoff at the entrance to ( $z = 0$ ) and exit from ( $z = L$ ) the medium. We express  $\psi(L, T, \tau) = \sqrt{g^{(2)}(\tau)}e^{i\phi_2(\tau)}$  and compare  $g^{(2)}(\tau)$  and  $\phi_2(\tau)$  found with three different methods: numerical simulations, EFT with no free parameters, and EFT with a uniform density with  $g_c$  a free

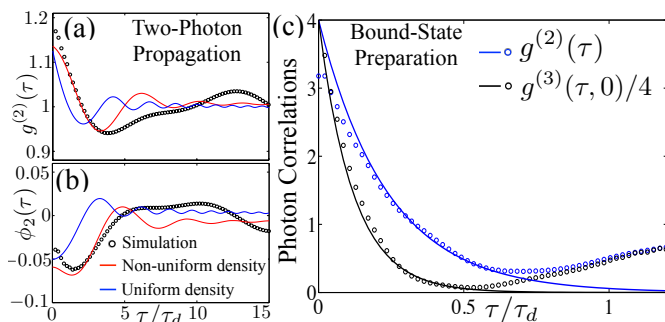


FIG. 2: (a,b) Two-photon transmission calculated using EFT (solid lines) and numerical simulations (circles). We took  $\Omega/2\pi = 5$  MHz,  $\Delta/2\pi = 20$  MHz,  $r_b = 10$   $\mu\text{m}$ ,  $OD = 10$ ,  $\sigma_{ax} = 36$   $\mu\text{m}$ ,  $L = 4\sigma_{ax}$ , and  $L' = 2.5\sigma_{ax}$ . To aid comparison we neglect decay from the  $|p\rangle$  and  $|s\rangle$  states. (b) Demonstration of two and three-body bound state preparation in numerical simulations (circles) for a uniform density with  $L = 430$   $\mu\text{m}$ ,  $OD = 300$ , and other parameters from (a). Solid lines are EFT predictions that only include the bound state contribution to the transmission.

parameter and medium length  $L'$  chosen to match the time delay  $\tau_d = \int_0^L dz [1/v_g(z)]$ . For  $\tau \lesssim \tau_d$ , both EFT results capture many of the qualitative features of the simulations, but the inhomogeneous EFT captures more features and obtains better quantitative agreement. At long times  $\tau \gg \tau_d$ , where the swap of time and space breaks down, the EFT deviates from the simulations.

For a long medium with a uniform density, we can find the transmission analytically

$$\psi(L, T, \tau) \approx 2e^{-\kappa|\tau| + iE_2^0\tau_d/\hbar} - \sqrt{\frac{\hbar/\pi}{|E_2^0|\tau_d}}(1 + \kappa|\tau|), \quad (6)$$

where  $E_2^0 = -\hbar^2/|m|a_2^2$  is the binding energy of the two-body bound state and we used a saddle point expansion, valid for  $|E_2^0|\tau_d/\hbar \gg (1 + \kappa|\tau|)$ . Equation (6) shows that the dispersive nature of the scattering states (second term) leads to their dephasing near the origin. For large  $\kappa|\tau|$ , the scattering states recover the boundary condition  $\lim_{\tau \rightarrow \infty} g^{(2)}(\tau) \rightarrow 1$ .

*Universal N-Body Bound States.*—For large scattering lengths ( $a_2 \gg r_b$ ) we can use Eq. (4) to study the transmission for photon numbers  $N > 2$  because all the renormalized parameters in the  $N$ -body sector are determined at the level of  $N = 2$  [22]. For attractive interactions, we now show that the  $N$ -photon transmission is dominated by the  $N$ -body bound states of Eq. (3). To see how this arises, note that these bound states are fundamentally related to the soliton solutions that emerge in the mean field limit of Eq. (4) [28, 29]. Similar to solitons, they propagate without distortion, which leads to their emergence over the background of scattering states.

For every  $N$ , the EFT has a single  $N$ -body bound state with a binding energy  $E_N^0 = E_2^0 N(N^2 - 1)/6$  and charac-

teristic radius  $R_N = \hbar(-|m|E_N^0)^{-1/2} \approx a_2 N^{-3/2}$  [31, 32]. The argument leading to Eq. (6) generalizes to these  $N$ -body bound states. We move from the original coordinates for the  $N$  polaritons ( $t_1, \dots, t_N$ ) to  $T = \sum_i t_i/N$  and a relative coordinate system  $\tau_1, \dots, \tau_{N-1}$  (defined as any orthogonal set to  $T$  [33]). We take the probe to be on two-photon resonance so that the  $N$ -polariton wavefunction  $\psi(z, T, \boldsymbol{\tau})$  satisfies  $\partial_T \psi = 0$ . The general form for the evolution for a uniform medium is [34]

$$\begin{aligned} \psi(z, T, \boldsymbol{\tau}) &= c_b(0)\psi_b(\boldsymbol{\tau})e^{iE_N z/\hbar v_g} \\ &+ \int \frac{d\omega}{2\pi} c_{b\omega}(0)\psi_{b\omega}(\boldsymbol{\tau})e^{iE_{N-1} z/\hbar v_g + i\hbar\omega^2 z/|m|v_g^3} + \dots, \end{aligned} \quad (7)$$

where  $\psi_b(\boldsymbol{\tau}) \propto (\frac{v_g}{R_N})^{\frac{N-1}{2}} e^{-\kappa \sum_{i < j} |t_i - t_j|}$  is the wavefunction for the  $N$ -body bound state [31, 32],  $\psi_{b\omega}(\boldsymbol{\tau})$  is the wavefunction for a combined  $(N-1)$ -body bound state and a scattering state with relative frequency  $\omega$ , etc. The non-bound contributions to  $\psi$  disperse near the origin and the bound state dominates the transmission there.

This effect is demonstrated in Fig. 2(b) using numerical simulations of the exact two and three-body wavefunction transmission through a long medium with a uniform density [26]. In the case of three photons, we express the transmitted field  $\psi(L, \tau_1, \tau_2) = \sqrt{g^{(3)}(\tau_1, \tau_2)}e^{i\phi_3(\tau_1, \tau_2)}$ . Consistent with EFT,  $g^{(2)}(\tau)$  takes the form of the two-body bound state near  $\tau = 0$  with the decay rate  $2\kappa$  and  $g^{(2)}(0) \approx |c_b(0)\psi_b(0)|^2 = 4$ . Similarly  $g^{(3)}(\tau, 0)$  has the decay rate of the three-body bound state  $4\kappa$  and  $g^{(3)}(0, 0) \approx |c_b(0)\psi_b(0, 0)|^2 = 16$ .

The length used in Fig. 2(b) would be difficult to realize experimentally without additional focusing or waveguiding for the probe light; however, as can be seen in Fig. 2(a) for the two-body problem, the same qualitative effects appear in much shorter media [4]. Finally, we remark that it is possible to prepare these bound states in media with a non-uniform density, provided the exit from the medium is not adiabatic. For an adiabatic exit, the bound state becomes progressively larger until it is indistinguishable from a uniform field.

*N-body Interactions.*—Strong long-range Rydberg interactions that result in blockade can also induce effective  $N$ -body interactions [35, 36]. For Rydberg polaritons, this is illustrated at the three-body level because, when two polaritons are less than  $r_b$  from a Rydberg atom, they do not interact with each other, leading to a three-body force with the opposite sign from the two-body force. For dimensions  $d < 3$ , these corrections are non-universal and generically result in perturbative corrections to the EFT [20, 22]. We now explicitly derive the  $N$ -body interaction potentials for Rydberg polaritons in 1d and show that they lead to large corrections to the binding energies of the bound states.

Effective  $N$ -body interactions emerge from integrating out virtual processes with high energy or large momenta. Conveniently, for Rydberg polaritons, the theory

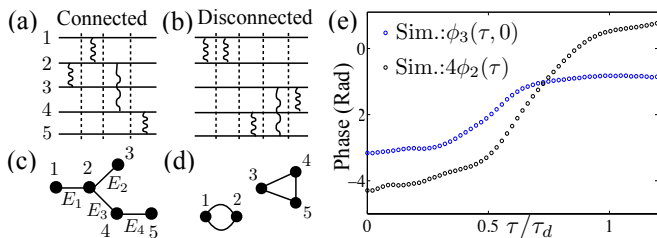


FIG. 3: Examples of a (a) connected and (b) disconnected scattering diagram for  $N = 5$ . The diagram in (a) contributes to  $V_{\text{eff}}^N$ , while (b) does not. (c,d) Graph representations of (a,b), respectively, neglecting the ordering of scattering events. The graph in (c) is a tree graph, which implies that (a) is a lowest order diagram for  $V_{\text{eff}}^N$ . (e) Phase of the transmitted two and three photon bound state from Fig. 2(b);  $h_3$  can be directly extracted from  $\phi_3(0, 0)$  and  $\phi_2(0)$ .

dramatically simplifies at large momenta because the single body propagator for the  $s$ -states saturates to its value for  $g_c = 0$ :  $\hbar\chi(\nu) = (\Delta + \nu)/[(\Delta + \nu)\nu - \Omega^2]$  [26]. The physical origin of this can be seen in Eq. (1), where the local momentum  $q(\omega, z)$  diverges at the Raman resonance conditions  $\Omega^2 - \omega(\Delta + \omega) = 0$ . These Raman excitations have a frequency close to two-photon resonance and effectively infinite mass; therefore, near  $\nu = 0$ , they dominate virtual processes with large internal momentum.

The  $N$ -body interaction potential  $V_{\text{eff}}^N$  arises from virtual processes where all  $N$  particles exchange momentum. These contributions to the scattering amplitudes are represented by connected diagrams of the type shown in Fig. 3(a), where the particles cannot be broken into disjoint clusters. Particles are connected by two-body interactions (curly lines), with the insertion of the  $N$ -body propagator in between (vertical lines). Figure 3(b) shows an example of a disconnected diagram, which is separable into two disjoint clusters (12) and (345) and does not contribute to  $V_{\text{eff}}^N$ .

Integral equations for the connected contributions to multi-particle scattering amplitudes were first formulated by Weinberg [37] and Rosenberg [38]. The full integral equations have only been solved for  $N \leq 4$  [33]; however, the problem is simplified for the constant (i.e., momentum independent) propagator described above. The local nature of the propagator implies that the ordering of the scattering events is irrelevant. In this limit, we can represent any scattering diagram by a graph of the type shown in Fig. 3(c,d), where the vertices correspond to particles and the edges indicate interaction pairs. Diagrams that map to a tree graph [e.g., Fig. 3(a,c)] give the lowest order contribution to  $V_{\text{eff}}^N$

$$V_{\text{eff}}^N(\mathbf{z}; \nu) \approx (N-1)! [\chi_N(\nu)]^{N-2} \sum_{T(N,E)} V_{E_1} \dots V_{E_{N-1}}, \quad (8)$$

where  $E_k = ij$ ,  $V_{E_k} = V(z_i - z_j)$ , and the sum is over all

labeled tree graphs  $T(N, E)$  with  $N$  vertices and  $N-1$  edges  $E = \{E_1, \dots, E_{N-1}\}$ . Here the  $N$ -body propagator is  $\hbar\chi_N(\nu) = \hbar^2 \int d\omega \chi(\omega) \chi_{N-1}(\nu - \omega) \approx (\nu - N\Omega^2/\Delta)^{-1}$  (for  $\Omega \ll \Delta$ ). For  $r \ll r_b$ , we have  $|V(r)\chi_N| > 1$ , and Eq. (8) is no longer valid. In the supplemental material, we derive the non-perturbative solution for  $V_{\text{eff}}^N$  [26].

We can also include non-perturbative effects in Eq (8) by replacing  $V(r)$  with the renormalized two-body interaction  $U(\tau) = -(2\hbar^2\kappa/mv_g^2)\delta(\tau)$ . In this case, the  $N$ -body interactions are contact forces. The resulting EFT is governed by Eq. (4) with

$$\mathcal{H} = \hat{\psi}^\dagger \left[ -i\hbar\partial_t - \frac{\hbar^2\partial_t^2}{2mv_g^2} \right] \hat{\psi} + \sum_N h_N \hat{\psi}^{\dagger N} \hat{\psi}^N, \quad (9)$$

$$h_N = \frac{(-1)^{N-1}}{N} \left( \frac{2\hbar^2\kappa}{mv_g^2} \right)^{N-1} (N\chi_N)^{N-2}, \quad (10)$$

where we used Cayley's tree formula  $N^{N-2}$  for the number of labeled tree graphs with  $N$  vertices in evaluating Eq. (8) [39]. Consistent with the blockade effects described above,  $h_3$  has the opposite sign from  $h_2$ . More generally,  $h_N$  and  $V_{\text{eff}}^N$  alternate with  $N$  between attraction and repulsion [26]. For weak interactions  $a_2 \approx (3/\pi)r_b/\varphi^2$  and Eq. (9) reduces to a perturbative expansion in the nonlinear phase shift  $\varphi$  introduced in the introduction. In the renormalized EFT, where only the first order correction in  $r_b/a_2 = (3/\pi)\varphi^2$  should be included, the  $N$ -body interactions are dropped for  $N \geq 3$  and the EFT reduces to our previous result in Eq. (3).

The Hamiltonian-like object in Eq. (9) can be used to study few- and many-body physics of Rydberg polaritons going beyond Eq. (3). For example, Eq. (9) predicts a correction to the  $N$ -body binding energy ( $N \geq 3$ )

$$\delta E_N \approx N! h_N |\psi_b(0, \dots, 0)|^2. \quad (11)$$

This energy shift can be measured by comparing the phase of the transmitted  $N$ -body bound state to the phase of the  $(N-1)$ -body bound state. This is illustrated in Fig. 3(e), which shows  $\phi_3(\tau, 0)$  for the transmitted state from Fig. 2(b). The deviation of  $\phi_3(0, 0)$  from the unperturbed value of  $4\phi_2(0) \approx E_3^0\tau_d/\hbar$  is a direct measurement of  $\delta E_3\tau_d/\hbar$ . We predict a large correction  $\delta E_3^{\text{EFT}}/|E_3^0| = 0.271$ , which is within 3% of the value extracted from Fig. 3(e)  $\delta E_3^{\text{Sim}}/|E_3^0| = 0.263$ . For  $\varphi \ll 1$ , Eq. (11) predicts the scaling  $\delta E_N/|E_N^0| \sim (r_b/R_N)^{N-1}$ . In particular, when the internal bound state momentum  $k \approx 1/R_N$  approaches  $1/r_b$ , the perturbative corrections from  $h_N$  become order one, signaling the breakdown of the EFT description. For parameters from recent experiments [4], this crossover occurs for  $N \gtrsim 5$ , past which, the  $N$ -body bound states sensitively depend on the microscopic details of the interactions.

*Outlook.*—We have constructed an EFT to describe non-perturbative  $N$ -body scattering of Rydberg polaritons in an atomic medium. We generally find good agreement between the predictions of this EFT and numerical

simulations of the exact two and three photon transmission. Rydberg polariton experiments can involve complex geometries [40] or more Rydberg levels [11], dimensions [41], and external control fields [42]. The theoretical methods developed here can be naturally extended to these more complex configurations. The ability to control and probe  $N$ -body interactions may lead to insights into the transition from few- to many-body physics, as well as new phases of strongly-correlated light and matter.

*Note.*—During completion of this work, we became aware of related work on the three-body problem for Rydberg polaritons [43].

*Acknowledgements.*—We thank I. Carusotto, O. Firstenberg, R. Qi, and M. Maghrebi for helpful discussion. This research was supported in part by the National Science Foundation under Grant No. NSF PHY11-25915, the NSF PFC at the JQI, the Harvard-MIT CUA, ARL CDQI, NSF QIS, AFOSR, and ARO.

- 
- [1] J. D. Pritchard, D. Maxwell, A. Gauguet, K. J. Weatherill, M. P. A. Jones, and C. S. Adams, *Phys. Rev. Lett.* **105**, 193603 (2010).
- [2] D. Petrosyan, J. Otterbach, and M. Fleischhauer, *Phys. Rev. Lett.* **107**, 213601 (2011).
- [3] A. V. Gorshkov, J. Otterbach, M. Fleischhauer, T. Pohl, and M. D. Lukin, *Phys. Rev. Lett.* **107**, 133602 (2011).
- [4] O. Firstenberg, T. Peyronel, Q.-Y. Liang, A. V. Gorshkov, M. D. Lukin, and V. Vuletić, *Nature* **502**, 71 (2013).
- [5] T. Peyronel, O. Firstenberg, Q.-Y. Liang, S. Hofferberth, A. V. Gorshkov, T. Pohl, M. D. Lukin, and V. Vuletić, *Nature* **488**, 57 (2012).
- [6] Y. O. Dudin and A. Kuzmich, *Science* **336**, 887 (2012).
- [7] D. Maxwell, D. J. Szwer, D. Paredes-Barato, H. Busche, J. D. Pritchard, A. Gauguet, K. J. Weatherill, M. P. A. Jones, and C. S. Adams, *Phys. Rev. Lett.* **110**, 103001 (2013).
- [8] H. Gorniaczyk, C. Tresp, J. Schmidt, H. Fedder, and S. Hofferberth, *Phys. Rev. Lett.* **113**, 053601 (2014).
- [9] D. Tiarks, S. Baur, K. Schneider, S. Dürr, and G. Rempe, *Phys. Rev. Lett.* **113**, 053602 (2014).
- [10] H. Gorniaczyk, C. Tresp, P. Bienias, A. Paris-Mandoki, W. Li, I. Mirgorodskiy, H. P. Büchler, I. Lesanovsky, and S. Hofferberth, arXiv:1511.09445 (2015).
- [11] D. Tiarks, S. Schmidt, G. Rempe, and S. Dürr, arXiv:1512.05740 (2015).
- [12] P. Bienias, S. Choi, O. Firstenberg, M. F. Maghrebi, M. Gullans, M. D. Lukin, A. V. Gorshkov, and H. P. Büchler, *Phys. Rev. A* **90**, 053804 (2014).
- [13] M. F. Maghrebi, M. J. Gullans, P. Bienias, S. Choi, I. Martin, O. Firstenberg, M. D. Lukin, H. P. Büchler, and A. V. Gorshkov, *Phys. Rev. Lett.* **115**, 123601 (2015).
- [14] O. Firstenberg, C. S. Adams, and S. Hofferberth, arXiv:1602.06117 (2016).
- [15] J. Otterbach, M. Moos, D. Muth, and M. Fleischhauer, *Phys. Rev. Lett.* **111**, 113001 (2013).
- [16] M. Moos, M. Höning, R. Unanyan, and M. Fleischhauer, *Phys. Rev. A* **92**, 053846 (2015).
- [17] A. Grankin, E. Brion, E. Bimbard, R. Boddeda, I. Usmani, A. Ourjoumtsev, and P. Grangier, *Phys. Rev. A* **92**, 043841 (2015).
- [18] See, e.g., H. Georgi, *Ann. Rev. Part. Sci.* **43**, 209 (1994).; D. B. Kaplan, arXiv:nucl-th/0510023 (2005).; C. P. Burgess, *Ann. Rev. Part. Sci.*, **57**, 329 (2007).
- [19] H. W. Hammer, *J. Phys. G: Nucl. Part. Phys.* **31**, S1253 (2005).
- [20] E. Braaten and H. W. Hammer, *Phys. Rep.* **428**, 259 (2006).
- [21] E. Braaten and A. Nieto, *Phys. Rev. B* **56**, 14 745 (1997); *Phys. Rev. B* **55**, 8090 (1997).
- [22] S. K. Adhikari, T. Frederico, and I. D. Goldman, *Phys. Rev. Lett.* **74**, 487 (1995).
- [23] P. F. Bedaque, H.-W. Hammer, and U. van Kolck, *Phys. Rev. Lett.* **82**, 463 (1999).
- [24] M. Fleischhauer, A. Imamoglu, and J. P. Marangos, *Rev. Mod. Phys.* **77**, 633 (2005).
- [25] More precisely, we define  $r_b$  via  $V(r_b) = \hbar/|\chi_2(0)| = 2\hbar\Omega^2|\Delta|/|\Omega^2 - \Delta^2|$  [12]. For our parameters, this definition is nearly equivalent to the one given in the main text.
- [26] See Supplemental Material for a derivation of the spatially varying scattering length, discussion of the numerical methods, and the non-perturbative solution for  $V_{\text{eff}}^N$ .
- [27] In the definition of  $m(z)$  below Eq. (1), we neglected a small correction of order  $\Omega^2/[g_c(z)]^2$ .
- [28] Y. Lai and H. A. Haus, *Phys. Rev. A* **40**, 844 (1989).
- [29] Y. Lai and H. A. Haus, *Phys. Rev. A* **40**, 854 (1989).
- [30] P.-É. Larré and I. Carusotto, *Eur. Phys. J. D* **70**, 1 (2016).
- [31] E. H. Lieb and W. Liniger, *Phys. Rev.* **130**, 1605 (1963).
- [32] J. B. McGuire, *J. Math. Phys.* **5**, 622 (1964).
- [33] S. K. Adhikari and K. L. Kowalski, *Dynamical Collision Theory and Its Applications* (Academic Press, San Diego, CA, 1991).
- [34] Y. Ben-Aryeh, *J. Opt. B: Quantum Semiclass. Opt.* **1**, 234 (1999).
- [35] H. P. Büchler, A. Micheli, and P. Zoller, *Nat Phys* **3**, 726 (2007).
- [36] H. Weimer, M. Müller, I. Lesanovsky, P. Zoller, and H. Büchler, *Nature Phys.* **6**, 382 (2010).
- [37] S. Weinberg, *Phys. Rev.* **133**, B232 (1964).
- [38] L. Rosenberg, *Phys. Rev.* **140**, B217 (1965).
- [39] R. P. Stanley, *Enumerative Combinatorics, Volume 1* (Cambridge Univ. Press, Cambridge, 2011), 2nd ed.
- [40] A. Sommer, H. P. Büchler, and J. Simon, arXiv:1506.00341 (2015).
- [41] S. Sevinçli, N. Henkel, C. Ates, and T. Pohl, *Phys. Rev. Lett.* **107**, 153001 (2011).
- [42] D. Maxwell, D. J. Szwer, D. Paredes-Barato, H. Busche, J. D. Pritchard, A. Gauguet, M. P. A. Jones, and C. S. Adams, *Phys. Rev. A* **89**, 043827 (2014).
- [43] K. Jachymski, P. Bienias, H. P. Büchler, arXiv:1604.03743 (2016).

## Supplemental Material

### Microscopic Model

In this section, we derive the two-body Lippmann-Schwinger equation for an inhomogeneous density and show that the spatially varying scattering length  $a_2(z)$  is well defined when the density varies slowly compared to the blockade radius.

The effective Hamiltonian, including decay, that describes the Rydberg polariton system is ( $\hbar = 1$ )

$$H = -ic \int dz \hat{\mathcal{E}}^\dagger(z) \partial_z \hat{\mathcal{E}}(z) \quad (\text{S1})$$

$$- \int dz g_c(z) [\hat{\mathcal{P}}(z) \hat{\mathcal{E}}^\dagger(z) + h.c.] + H_p + H_{\text{int}},$$

$$H_p = - \int dz (\Delta + i\gamma) \hat{\mathcal{P}}^\dagger(z) \hat{\mathcal{P}}(z) \quad (\text{S2})$$

$$- i\gamma_s \hat{\mathcal{S}}^\dagger(z) \hat{\mathcal{S}}(z) - \Omega [\hat{\mathcal{P}}^\dagger(z) \hat{\mathcal{S}}(z) + h.c.],$$

$$H_{\text{int}} = \int dz dz' V(z - z') \hat{\mathcal{S}}^\dagger(z) \hat{\mathcal{S}}^\dagger(z') \hat{\mathcal{S}}(z') \hat{\mathcal{S}}(z), \quad (\text{S3})$$

where  $\hat{\mathcal{E}}(z)$ ,  $\hat{\mathcal{P}}(z)$ , and  $\hat{\mathcal{S}}(z)$  are bosonic annihilation operators for a photon, excited atom, and Rydberg state at position  $z$ . They satisfy  $[\hat{\mathcal{E}}(z), \hat{\mathcal{E}}^\dagger(z')] = [\hat{\mathcal{P}}(z), \hat{\mathcal{P}}^\dagger(z')] = [\hat{\mathcal{S}}(z), \hat{\mathcal{S}}^\dagger(z')] = \delta(z - z')$ . The parameters  $\Delta$ ,  $\Omega$ ,  $\gamma$ , and  $g_c(z)$  are defined in the main text and  $\gamma_s$  is the halfwidth of the  $s$ -state.

For an inhomogeneous medium it is convenient to solve the scattering problem in real space. For a single polariton we can find the propagator at frequency  $\omega$  from the equations of motion

$$-i\omega E(z) = -c\partial_z E + ig_c(z)P(z), \quad (\text{S4})$$

$$-i\omega P(z) = -(\gamma - i\Delta)P(z) + ig_c(z)E(z) + i\Omega S(z), \quad (\text{S5})$$

$$-i\omega S(z) = -\gamma_s S(z) + i\Omega P(z). \quad (\text{S6})$$

The solution is given by

$$E_\omega(z, z_0) = \frac{1}{N_\omega(z)} \exp \left[ i \int_{z_0}^z dz' q(\omega, z') \right], \quad (\text{S7})$$

$$q(\omega, z) = \frac{\omega}{c} \left( 1 - \frac{[g_c(z)]^2}{\tilde{\Delta}\tilde{\delta}} \right), \quad (\text{S8})$$

$$P_\omega(z, z_0) = -\frac{g_c(z)}{\tilde{\Delta}} \left( 1 + \frac{\Omega^2}{\tilde{\Delta}\tilde{\delta}} \right) E_\omega(z, z_0), \quad (\text{S9})$$

$$S_\omega(z, z_0) = \frac{g_c(z)\Omega}{\tilde{\Delta}\tilde{\delta}} E_\omega(z, z_0), \quad (\text{S10})$$

where  $\tilde{\Delta} = \Delta + \omega + i\gamma$ ,  $\tilde{\delta} = -\Omega^2/\tilde{\Delta} + \omega + i\gamma_s$ ,  $N_\omega(z)$  is a normalization constant chosen to satisfy  $|E_\omega(z)|^2 + |P_\omega(z)|^2 + |S_\omega(z)|^2 = 1$ , and  $q(\omega, z)$  is defined in Eq. (1) in the main text for  $\gamma = \gamma_s = 0$ .

To each of these wavefunctions, we associate the operator

$$\hat{\psi}_\omega^\dagger(z_0) = \int dz \sqrt{\rho(\omega, z_0)} [E_\omega(z, z_0) \hat{\mathcal{E}}^\dagger(z) + P_\omega(z, z_0) \hat{\mathcal{P}}^\dagger(z) + S_\omega(z, z_0) \hat{\mathcal{S}}^\dagger(z)]. \quad (\text{S11})$$

where  $\rho(\omega, z_0) = dq(\omega, z_0)/d\omega$  is the local density of states. For an infinite, homogeneous medium this operator creates a dark-state polariton [24]. For a sufficiently slowly varying density, this field becomes approximately bosonic with the commutation relation

$$[\hat{\psi}_\omega(z_0), \hat{\psi}_{\omega'}^\dagger(z_0)] = \int dz \rho(\omega, z_0) e^{i \int_{z_0}^z dz' [q(\omega, z') - q(\omega', z')]} \approx \rho(\omega, z_0) \delta[q(\omega, z_0) - q(\omega', z_0)] = \delta(\omega - \omega'). \quad (\text{S12})$$

When  $\omega$  is on the Raman resonance  $\tilde{\Delta}\tilde{\delta} = 0$ , these solutions need to be treated with care because  $E_\omega \rightarrow 0$  and these states do not propagate. The Raman resonance condition

$$\tilde{\Delta}\tilde{\delta} = (\omega + i\gamma_s)(\Delta + \omega + i\gamma) - \Omega^2 = 0 \quad (\text{S13})$$

has the solutions

$$\omega_\pm = -\frac{\Delta + i(\gamma + \gamma_s)}{2} \pm \sqrt{\frac{[\Delta + i(\gamma + \gamma_s)]^2}{4} + \Omega^2 + (\gamma - i\Delta)\gamma_s}. \quad (\text{S14})$$

We work in the limit of large  $\Delta$  and small  $\gamma_s$ , where these resonances can be treated as if they were on the real axis. For these two eigenstates,  $\hat{\psi}_\pm^\dagger(z_0) = P_\pm \hat{\mathcal{P}}^\dagger(z_0) + S_\pm \hat{\mathcal{S}}^\dagger(z_0)$  with

$$P_\pm = \frac{\omega_\pm}{\sqrt{\Omega^2 + \omega_\pm^2}}, \quad (\text{S15})$$

$$S_\pm = \frac{\Omega}{\sqrt{\Omega^2 + \omega_\pm^2}}. \quad (\text{S16})$$

To solve the interacting problem, Eq. (S3) implies that we only need the propagator projected onto the Rydberg states. We can use the eigenstates  $\hat{\psi}_\omega^\dagger(z_0)|0\rangle$  to find the propagator in a vicinity of  $z_0$

$$g_0^{ss}(z, z_0, \nu) = \langle \hat{S}(z) \frac{1}{\nu - H_0 + i0^+} \hat{S}^\dagger(z_0) \rangle \quad (\text{S17})$$

$$= \int d\omega \frac{\langle \hat{S}(z) \hat{\psi}_\omega^\dagger(z_0) \rangle \langle \hat{\psi}_\omega(z_0) \hat{S}^\dagger(z_0) \rangle}{\nu - \omega + i0^+} = \rho(\nu, z_0) S_\nu(z, z_0) S_\nu^*(z_0, z_0) + \chi(\nu) \delta(z - z_0),$$

$$\chi(\nu) = \sum_{s=\pm} \frac{|S_s|^2}{\nu - \omega_s} = \frac{\Delta + \nu}{(\Delta + \nu)\nu - \Omega^2}. \quad (\text{S18})$$

As discussed in the main text, the  $\chi(\nu)$  contribution arises from the two Raman resonances and accounts for the saturation of the propagator at large momentum.

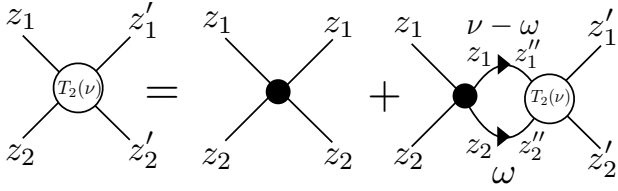


FIG. S1: Diagrammatic representation of the two-body Lippmann-Schwinger equation in real space,  $\nu$  is the total frequency of the two polaritons, dots are  $V(z_1 - z_2)$ , and the lines are the single-polariton propagator  $g_0^{ss}(z, z', \nu)$ .

With this representation of the single particle propagator, we can now write down the explicit Lippmann-Schwinger equation for the transition matrix for Rydberg polaritons in an inhomogeneous medium, represented diagrammatically in Fig. S1,

$$T_2(\mathbf{z}, \mathbf{z}', \nu) = V(z_1 - z_2) [\delta(\mathbf{z} - \mathbf{z}') \quad (\text{S19})$$

$$+ \int d\mathbf{z}'' g_0^{ss,ss}(\mathbf{z}, \mathbf{z}'', \nu) T_2(\mathbf{z}'', \mathbf{z}', \nu)],$$

$$g_0^{ss,ss}(\mathbf{z}, \mathbf{z}'', \nu) = \int d\omega g_0^{ss}(z_1, z_1'', \omega) g_0^{ss}(z_2, z_2'', \nu - \omega). \quad (\text{S20})$$

To find the EFT parameters, we replace  $g_0^{ss}(z_1, z_1'', \omega)$  with the first term in the last line of Eq. (S17) and approximate the dispersion by the formula given below Eq. (1) in the main text  $\omega = v_g(z)q + q^2/2m(z)$ . We then replace  $V(z_1 - z_2)$  with the pseudopotential  $-2\hbar^2\delta(r)/m(z)a_2(z)$ , where  $z = (z_1 + z_2)/2$  and  $r = z_1 - z_2$  and derive an effective solution for  $T_2$ . This can then be matched to the asymptotic solution for the exact  $T_2$ . When the propagator varies slowly with  $z$  compared to the potential (i.e., the density changes slowly on the scale of  $r_b$ ), we can find the  $T_2$  using the approach of Ref. [12] for a uniform density. All the results presented in the main text are in the weakly interacting regime with attractive interactions, where  $a_2(z) \approx 3r_b/\pi[\varphi(z)]^2$  [12].

### Numerical Methods

In this section, we detail the numerical methods used in the simulations for Fig. 2 and Fig. 3 in the main text.

The numerical simulations used in Fig. 2 and Fig. 3 in the main text solve the Schrödinger equation, with  $H$  given by Eq. (S1), for the two and three-body wavefunction. We solve the propagation in steady state with a split-operator approach described in Ref. [13]. We write  $H$  as a sum of the kinetic and potential terms and evolve them separately in a Trotter decomposition. Such an approach is efficient because only the first term in Eq. (S1) is not diagonal in real space. For a time step  $\Delta t$ , this term simply advances the wavefunction uniformly by  $c\Delta t$

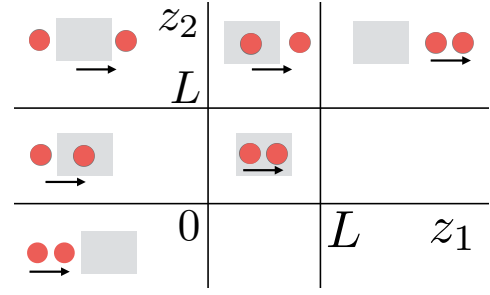


FIG. S2: Distinct regions of phase space for the two-photon wavefunction;  $z_1$  and  $z_2$  are the coordinates of the two photons. Diagram within each region depicts the spatial configuration of the photons (red circles) in that region; grey rectangle denotes the atomic medium, while arrow indicates propagation direction.

and does not require a Fourier transform to perform the propagation in momentum space.

To numerically solve the two-photon problem we need to propagate 9 wavefunction components  $\vec{\psi}(z_1, z_2) = (EE(z_1, z_2), \dots, SS(z_1, z_2))$ ; for three-photons, there are 27 components  $\vec{\psi} = (EEE, \dots, SSS)$ , etc. Here  $EP(z_1, z_2) = \langle 0 | \hat{\mathcal{E}}(z_1) \hat{\mathcal{P}}(z_2) | \psi \rangle$  and similarly for the other components. The propagation problem has two important simplifications. First, the input photonic state is symmetric, which implies that we only need to find the wavefunction in the region  $z_1 < \dots < z_N$  (e.g., see Fig. S2). Second, a large fraction of the components are non-propagating and can be expressed locally in terms of the propagating components. For two photons, the non-propagating components are  $PP$ ,  $PS$ ,  $SP$ , and  $SS$ , while for three photons there are 8 such components:  $(PPP, \dots, SSS)$ . Let  $P_{\text{np}}$  be the projector into the space of non-propagating states, then

$$\omega P_{\text{np}} \vec{\psi} = P_{\text{np}} H [P_{\text{np}} + (I - P_{\text{np}})] \vec{\psi}. \quad (\text{S21})$$

By construction this equation contains no  $z$  derivatives, so it can be directly inverted to express the non-propagating states in terms of the propagating ones

$$P_{\text{np}} \vec{\psi} = \frac{1}{\omega - P_{\text{np}} H} P_{\text{np}} H (I - P_{\text{np}}) \vec{\psi}. \quad (\text{S22})$$

This equation greatly simplifies the numerical treatment of this propagation problem for multi-level atoms.

To avoid the extraneous use of computational resources in regions with a very low, or zero, density, we treat the entrance and exit into the atomic medium as distinct boundaries [5]. The structure of this boundary problem for two photons is shown in Fig. S2. The bottom left of this diagram corresponds to the input region where the initial state is taken to be completely uniform. This sets the boundaries for the two regions with one photon in and one behind, etc. In addition, each region

has a different number of excitations within the medium, which determines the equations of motion through projections of Eq. (S1). The same approach to the boundary problem applies for the three-photon case; however, instead of 6 distinct regions under permutation of the photons, there are 10 regions. More generally, for  $N$  photons, the number of distinct regions is equivalent to the number of distinct strings with  $N$  zeros and two ones (where the one corresponds to inserting one of the two boundaries of the medium in between the photons):  $\binom{N+2}{2} = (N+2)(N+1)/2$ .

Finally, there is a large mismatch between the group velocity inside the medium  $v_g$  and the speed of light  $c$ ,

$$v_g/c = \Omega^2/g_c^2 \sim 10^{-6}. \quad (\text{S23})$$

This implies that regions such as the top-middle in Fig. (S2) are difficult to treat because of the large separation of scales between the propagation outside the medium versus inside. For every advance of the polariton inside the medium by one step, the photon outside advances roughly  $10^6$  steps. To speed up this process, we employ the scaling transformation  $z \rightarrow z\zeta$  and  $g_c(z) \rightarrow g_c(z\zeta)/\sqrt{\zeta}$  so that the group delay and optical depth per blockade radius stay constant, but  $v_g/c \rightarrow v_g\zeta/c$ . In Ref. [13], it was shown that the solutions to the two-photon problem remain invariant under this transformation provided  $v_g\zeta/c \ll 1$ . In Fig. 2(a-b) and Fig. 3(b) in the main text we use  $\zeta = 10^3$ .

### Non-Perturbative $N$ -body Interaction Potential

When  $|\chi_N V(r)| > 1$ , the perturbative solution for  $V_{\text{eff}}^N$  given in Eq. (8) of the main text breaks down. We now show how to find the non-perturbative solution to  $V_{\text{eff}}^N$  recursively using the Rosenberg integral equations for the connected transition matrix [38]. We explicitly solve these equations for  $N = 2, 3$ , and 4. Finally, we show that, inside the blockade radius,  $V_{\text{eff}}^N$  oscillates between attraction and repulsion with every increase in  $N$ .

Before writing the Rosenberg equations, we first introduce some basic concepts needed to describe  $N$ -particle scattering [33]. The notion of connected scattering diagrams, illustrated in Fig. 3 in the main text, leads to the cluster decomposition for the  $N$ -body transition matrix

$$T_N = \sum_{\alpha \in P} [T_N]_{\alpha}, \quad (\text{S24})$$

where  $P$  is the set of all partitions of  $N$  particles into disjoint clusters. For example, for three particles there are five such partitions (1)(2)(3), (12)(3), (13)(2), (23)(1), and (123). We define  $n_{\alpha}$  as the number of clusters within the partition  $\alpha$ . We denote the particles represented in each cluster as  $i_1, \dots, i_{m_n}$ , where  $1 \leq n \leq n_{\alpha}$  and  $m_n$  is the length of the  $n$ th cluster. For the partition

(12)(3)  $n_{\alpha} = 2$ ,  $m_1 = 2$  with  $i_1 = 1, i_2 = 2$  and  $m_2 = 1$  with  $i_1 = 3$ . We also introduce the notion of an ordering  $\prec$  of the clusters:  $\alpha \prec \beta$  if every cluster in  $\alpha$  is a subset of the elements in clusters of  $\beta$ . For example, (12)(3)(45)  $\prec$  (123)(456), but (12)(3)(45)  $\not\prec$  (1234)(56).

To find each term in Eq. (S24), one needs to evaluate the sum of all scattering diagrams where each cluster in the partition is disconnected from the others, but fully connected internally. For example, the diagram in Fig. 3(b) of the main text contributes to  $[T_N]_{\alpha}$  with  $\alpha = (12)(345)$ . In Eq. (8) of the main text we derived a perturbative solution for the fully connected contribution to  $T_N$ ,  $V_{\text{eff}}^N = [T_N]_{\alpha}$  with  $\alpha = (1, \dots, N)$ . However, this equation breaks down for  $r \ll r_b$  where  $|\chi_N V(r)| > 1$ . In this limit,  $V_{\text{eff}}^N$  has to be found non-perturbatively.

The key insight into the connected  $N$ -body scattering diagrams is that they can each be written as the product  $M_{\alpha}^{\ell} \chi_N L_{\ell}$ , where  $L_{\ell}$  is a diagram that ends with interaction  $V_{\ell}$  on the left and  $M_{\alpha}^{\ell}$  can be broken into two disjoint clusters  $\alpha$  such that  $\ell \not\prec \alpha$  [37, 38]. For the connected diagram in Fig. 3(a) in the main text  $M_{\alpha}^{\ell} = \chi_N^2 V_{12} V_{23} V_{24}$  and  $L_{\ell} = V_{45}$ , with  $\alpha = (1234)(5)$  and  $\ell = (45)$ . The Rosenberg integral equations (which are algebraic equations for a constant propagator) take advantage of this structure to recursively define [33, 38]

$$T_{N\ell}^c = \sum_{\ell'} \sum_{\alpha \succ \ell, n_{\alpha}=2} [T_{\ell}]_{\alpha} \bar{\Delta}_{\alpha\ell'} \chi_N T_{\ell'}, \quad (\text{S25})$$

$$T_N = \sum_{\ell} T_{\ell}, \quad (\text{S26})$$

$$T_{\ell} = V_{\ell} + V_{\ell} \chi_N T_N = \frac{V_{\ell}}{1 - \chi_N \sum_{\ell'} V_{\ell'}}, \quad (\text{S27})$$

$$V_{\text{eff}}^N(\mathbf{z}; \nu) = \sum_{\ell} T_{N\ell}^c(\mathbf{z}; \nu), \quad (\text{S28})$$

where  $\ell = ij$  ranges over all  $N(N-1)/2$  particle pairs (note, we changed notation from Eq. (8) in the main text),  $T_{\ell}$  groups all diagrams contributing to  $T_N$  that end with the interaction  $V_{\ell}$  on the left, and  $\nu$  is the total frequency of the incoming photons. The sum in Eq. (S25) is over all partitions  $\alpha$  with two clusters, which contain the pair  $\ell$ . The matrix  $\bar{\Delta}_{\alpha\ell'} = 1$  if  $\ell' \not\prec \alpha$  and zero otherwise.  $\bar{\Delta}_{\alpha\ell'}$  reflects the structure of the connected diagrams described above and enforces that all the terms in Eq. (S25) are fully connected. Equation (S25) is recursive because  $[T_{\ell}]_{\alpha}$  can be expressed in terms of the connected transition matrices for  $1 \leq k \leq N-2$

$$[T_{\ell}]_{\alpha} = T_{N-1, \ell}^{Nc}(z_{i_1}, \dots, z_{i_{N-1}}), \quad (k=1) \quad (\text{S29})$$

$$[T_{\ell}]_{\alpha} = \binom{N-3}{k-1} \chi_N T_{N-k, \ell}^{Nc}(z_{i_1}, \dots, z_{i_{N-k}}) \times \sum_{\ell' \prec (i_1 \dots i_k)} T_{k\ell'}^{Nc}(z_{i_1}, \dots, z_{i_k}), \quad (k > 1) \quad (\text{S30})$$

where the superscript  $N$  denotes that  $T_{m\ell}^{Nc}$  is found using Eq. (S25) for  $m$  particles, but with the propagator  $\chi_N$

replacing  $\chi_m$ . The binomial factor in front of Eq. (S30) counts the number of ways to arrange the scattering events between the two clusters, with the constraint that the pair  $\ell$  always interact first.

For  $N = 3$ , we find the non-perturbative solution

$$T_{3(12)}^c = \frac{\chi_3}{1 - \chi_3 \sum_{\ell} V_{\ell}} \frac{V_{12}}{1 - \chi_3 V_{12}} (V_{13} + V_{23}), \quad (\text{S31})$$

$$T_{3(13)}^c = \frac{\chi_3}{1 - \chi_3 \sum_{\ell} V_{\ell}} \frac{V_{13}}{1 - \chi_3 V_{13}} (V_{12} + V_{23}), \quad (\text{S32})$$

$$T_{3(23)}^c = \frac{\chi_3}{1 - \chi_3 \sum_{\ell} V_{\ell}} \frac{V_{23}}{1 - \chi_3 V_{23}} (V_{12} + V_{13}), \quad (\text{S33})$$

$$V_{\text{eff}}^3(z_1, z_2, z_3; \nu) = \sum_{\ell} T_{3\ell}^c(z_1, z_2, z_3; \nu), \quad (\text{S34})$$

which agrees with the perturbative result from Eq. (8) in the main text to lowest order in  $|\chi_3 V_{\ell}|$ . For  $N = 4$ , the full expression involves considerably more terms:

$$\begin{aligned} T_{4(12)}^c &= \frac{\chi_4}{1 - \chi_4 \sum_{\ell} V_{\ell}} [T_{3(12)}^{4c}(z_1, z_2, z_3)(V_{14} + V_{24} + V_{34}) \\ &\quad + T_{3(12)}^{4c}(z_1, z_2, z_4)(V_{13} + V_{23} + V_{34}) \\ &\quad + \chi_4 T_{2(12)}^{4c} T_{2(34)}^{4c}(V_{13} + V_{14} + V_{23} + V_{24})], \end{aligned} \quad (\text{S35})$$

and similarly for the other  $\ell$ . Here  $T_{3(12)}^{4c}(z_1, z_2, z_3)$  is given by  $T_{3(12)}^c(z_1, z_2, z_3)$  from Eq. (S31) with  $\chi_3(\nu)$  replaced by  $\chi_4(\nu)$ ,  $T_{2(12)}^{4c} = V_{12}/(1 - \chi_4 V_{12})$  and similarly for  $T_{3(12)}^{4c}(z_1, z_2, z_4)$  and  $T_{2(34)}^{4c}$ . The resulting expression for  $V_{\text{eff}}^4$ , to lowest order in  $\chi_4 V_{\ell}$ , contains 96 tree diagrams (16 unique) and agrees with Eq. (8) in the main text.

By construction, Eq. (S25) accounts for all connected scattering diagrams. To check that these recursive formulas give the same number of terms as the perturbative result, we use Eq. (S25)-(S30) to find a recursive formula for the number of terms contributing to  $T_{N\ell}^c$

$$t_2^{\ell} = 1, \quad (\text{S36})$$

$$t_N^{\ell} = t_{N-1}^{\ell} (N-2)(N-1) \quad (\text{S37})$$

$$+ \sum_{k=2}^{N-2} t_{N-k}^{\ell} t_k^{\ell} \frac{k(k-1)}{2} \binom{N-3}{k-1} \binom{N-2}{k} (N-k)k,$$

where  $\binom{N-2}{k}$  is the number two-cluster partitions containing  $\ell$  with  $m_1 = N - k$  and  $m_2 = k$  and  $(N - k)k$  is the number of non-zero elements in  $\bar{\Delta}_{\alpha\ell'}$  for each two-cluster partition  $\alpha$ . Based on Eq. (8) in the main text we expect  $t_N^{\ell} = 2(N-2)!N^{N-3}$ . This can be proved by induction using Eq. (S37) combined with an application of the binomial formula [39]

$$\frac{(a+b)^n}{a} = \sum_{k=0}^n \binom{n}{k} (a - kc)^{k-1} (b + kc)^{n-k}, \quad (\text{S38})$$

with  $a = 1$ ,  $c = -1$ ,  $b = N-1$ , and  $n = N-3$ . This result helps confirm that Eq. (8) of the main text is consistent with our non-perturbative solution for  $V_{\text{eff}}^N$ .

When all the photons are separated by much less than the blockade radius, we can approximate  $V(r)$  by  $\pm\infty$  and show by induction that

$$V_{\text{eff}}^N \approx (-1)^{N-1} \frac{N!N^{N-3}}{\chi_N}. \quad (\text{S39})$$

As a result, similar to the perturbative result from Eq. (10) in the main text,  $V_{\text{eff}}^N$  alternates between attraction and repulsion for every increase in  $N$ .